PROCEEDINGS OF SCIENCE

Elastic nucleon-deuteron scattering and breakup with chiral forces

Henryk Witała*, **Jacek Golak, Roman Skibiński, Kacper Topolnicki**†
M. Smoluchowski Institute of Physics, Jagiellonian University, PL-30348 Kraków
E-mail: henryk.witala@uj.edu.pl

Results on three-nucleon (3N) elastic scattering and breakup below the pion production threshold are discussed with an emphasis on the need for a three-nucleon force (3NF). The large discrepancies found between a theory based on numerical solutions of 3N Faddeev equations with (semi)phenomenological nucleon-nucleon (NN) potentials only and data point to the need for 3NF's. This notion is supported by the fact that another possible reason for the discrepancies in elastic nucleon-deuteron (Nd) scattering, relativistic effects, turned out to be small. Results for a new generation of chiral NN forces (up to N^4LO) together with theoretical truncation errors are shown. They support conclusions obtained with standard NN potentials

The 8th International Workshop on Chiral Dynamics
29 June 2015 - 03 July 2015
Pisa, Italy

*Speaker.

†This work was supported by the Polish National Science Center under Grant No. DEC-2013/10/M/ST2/00420. Some part of the work was performed within LENPIC collaboration. The numerical calculations have been performed on the supercomputer cluster of the JSC, Jülich, Germany.

PoS(CD15)122

1. Introduction

Traditionally in nuclear physics the Hamiltonian has been taken in a nonrelativistic form in which pairwise interactions between nucleons are supplemented by 3NF's for systems with more than two nucleons. The construction of NN potentials guided by a meson picture led to a generation of realistic NN interactions which described the NN data set with high precision (χ^2/datum $\approx$ 1) [1, 2, 3]. The 3N system is the first nontrivial case where those realistic potentials can be tested. In that system also for the first time 3NF's come into play making it a valuable source of information on 3NF properties and displaying their significance in the nuclear Hamiltonian.

The need for 3NF's was established when three- and four-nucleon bound states have been solved exactly. It was natural to look for an explanation of resulting underbinding introducing 3NF's such as the Urbana IX (UIX) [4] or the Tucson-Melbourne (TM) model [5] in the nuclear Hamiltonian.

Effective field theoretical methods in a form of chiral perturbation theory (χPT) provided a solid basis for a construction of nuclear forces. Consistent chiral NN [6, 7, 8] and 3N [9, 10, 11] forces have been derived in the χPT framework. Recently improved chiral NN potentials have been constructed by using appropriate regularization in the coordinate space [12, 13]. This significantly reduced finite-cutoff artefacts of the nonlocal momentum-space regulator used in [7, 8] allowing us to apply improved forces to higher energy Nd scattering.

In the next section we briefly review the 3N scattering formalism and give some examples where data are compared to various NN potential predictions alone or combined with different 3NF's. These examples are chosen to show the importance of the 3NF in the 3N system. The 3NF effects seem to grow with increasing energy of the 3N system. Therefore we discuss the importance of relativistic effects in elastic Nd scattering and their significance in the study of 3NF effects. The small size of relativistic effects indicates that one should focus on 3NF's, specifically of short-range nature. In the following section we present examples of results for improved chiral NN potentials. We summarize in the last section.

2. Reactions in the 3N continuum

All observables for elastic Nd scattering can be obtained from a state $T|\phi\rangle$ which fulfills the 3N Faddeev equation [14]

$$T|\phi\rangle = tP|\phi\rangle + (1+tG_0)V_4^{(1)}(1+P)|\phi\rangle + tPG_0T|\phi\rangle + (1+tG_0)V_4^{(1)}(1+P)T|\phi\rangle \ . \quad (2.1)$$

The initial channel state $|\phi\rangle$ is composed of a deuteron and a momentum eigenstate of the projectile nucleon. On a top of 2N forces with their off-the-energy shell t-matrix t for nucleons 2 and 3, also a 3NF is included and $V_4^{(1)}$ is the part of it which is symmetrical under the exchange of nucleons 2 and 3. The permutation operator P takes into account the identity of the nucleons and G_0 is the free 3N propagator.

Using the realistic NN forces: AV18 [1], CD Bonn [2], Nijm1, Nijm2, and Nijm93 [3] one gets in general predictions for 3N scattering observables which agree well with data at energies below $\approx$ 30 MeV. A fairly complete overview of those theoretical predictions in comparison to data is presented in [15, 16]. At higher energies discrepancies develop. They are exemplified for the nd

total and elastic scattering cross sections in Figures 1 and 2a, respectively. The large discrepancy between the theory and experimental data for the total cross section and in the minimum of the elastic scattering cross section obtained with NN forces only, seen for energies above ≈ 60 MeV, is removed for energies below ≈ 140 MeV when 3NF's, which reproduce the experimental triton binding energy, are included [17, 16] (see Figures 1b and 2a). A similar behavior shows up for the high energy deuteron vector analyzing power $A_y(d)$ [16]. But there are many spin observables for which large 3NF effects are predicted and where the TM and the Urbana IX do not reproduce the data [16]. This is the case e.g. for the nucleon analyzing power A_y [16] and for the deuteron tensor analyzing powers [16]. In none of these cases the data can be reproduced by pure 2N force predictions. Also in the deuteron breakup numerous spin observables were found which require 3NF's for their explanation [18, 19]. Therefore for elastic Nd scattering and deuteron breakup one can identify observables, which are sensitive to the structure of 3NF.

3. Relativistic effects in elastic Nd scattering

There are large discrepancies at higher energies between data and theory in elastic Nd scattering which cannot be removed by taking into account standard 3NF's (see Figure 2a). They require to study the magnitude of relativistic effects. We used an instant form relativistic approach which encompasses relativistic kinematics, boost corrections, and Wigner spin rotations [20, 21]. The boost effects turned out to be the most significant ones for the elastic scattering cross section at higher energies. They reduce the transition matrix elements at higher energies and lead, in spite of the increased relativistic phase-space factor as compared to the nonrelativistic one, to rather small effects in the cross section, mostly restricted to the backward angles [20] (see Figure 2b). Higher energy elastic scattering spin observables are only slightly modified by relativity [20, 21].

4. Results with chiral NN forces

The small size of relativistic effects indicates that very probably the short range contributions to the 3NF are responsible for the higher energy elastic scattering discrepancies. The recently constructed new generation of chiral NN potentials up to N^{4}LO with an appropriate regularization in the coordinate space [12, 13] made it possible to reduce significantly finite-cutoff artefacts present when using the nonlocal momentum-space regulator employed in the chiral NN potentials of Refs. [7, 8]. Such artefacts are clearly seen in strong variations around $p = 2$ fm^{-1} of the $l = 0$ component of the deuteron wave function calculated with N^{3}LO NN potentials of Refs. [7] and [8] (see Figures 3c and 3d). These variations are absent when new forces are used (see Figures 3g and 3h). Application of these new NN potentials does not lead to distortions in the cross section minimum of the higher energy elastic Nd scattering that were found in Ref. [22]. Also convergence with respect to the order of chiral expansion is improved when new chiral forces are applied, as exemplified in Figure 4 for the analyzing power A_y. At low energies of the incoming neutron, theoretical predictions of standard NN potentials fail to explain the experimental data for A_y (see Figure 4a). When instead of standard forces old chiral NN interactions with nonlocal momentum space regulator are used the predictions for A_y vary strongly with the order of chiral expansion. In particular, the NLO results overestimate the A_y data while N^{2}LO NN forces seem to provide quite

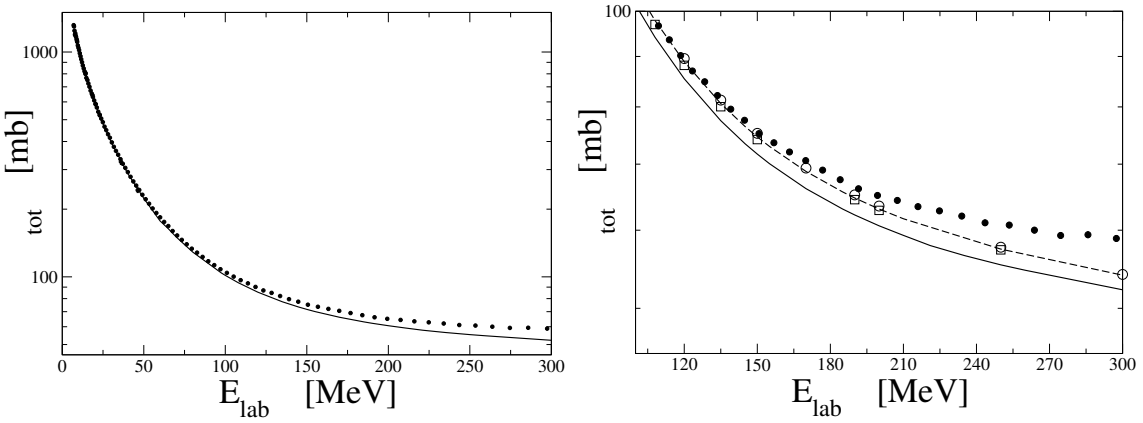

Figure 1: The neutron-deuteron total cross section as a function of the neutron lab. energy E_{lab}. The solid and dashed lines are the CD Bonn and CD Bonn+TM [5] 3NF predictions, respectively. The open squares and circles are the AV18+Urbana IX [4] 3NF and CD Bonn+TM99 [23] 3NF predictions, respectively. Solid dots are experimental data from [24].

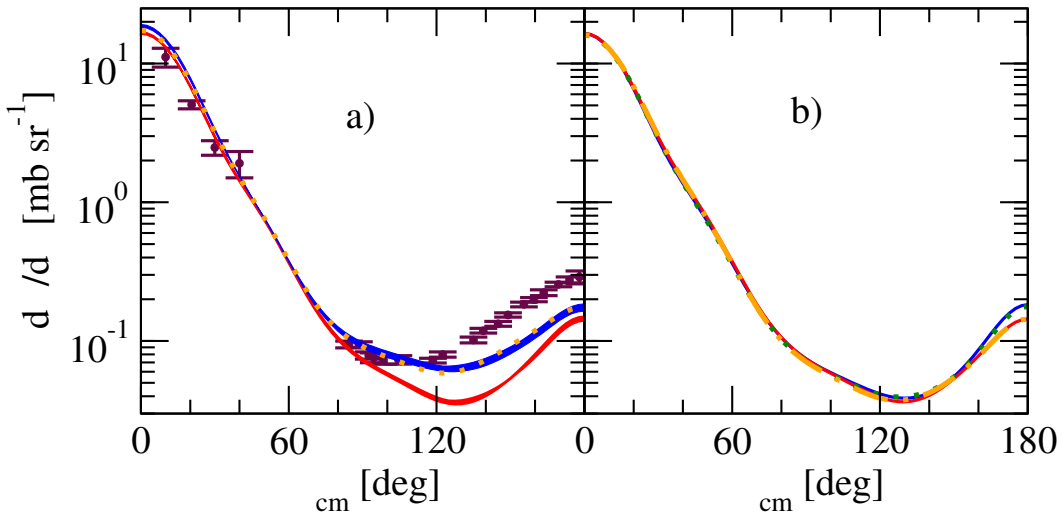

Figure 2: (Color online) The angular distribution for nd elastic scattering at neutron energy $E_{lab} = 250$ MeV. The nd experimental data (solid dots) are from [25]. In a) the light shaded (red) and dark shaded (blue) bands result from predictions of (semi)phenomenological potentials alone (AV18, CD Bonn, Nijm1, Nijm2) and combined with TM99 3NF, respectively. The dotted (orange) line is the prediction of the AV18+UIX 3NF. In b) the solid (red) and dashed-dotted (orange) line (they practically overlap) is the prediction of the CD Bonn and AV18 potential, respectively. The solid (blue) and the dotted (green) lines (also they practically overlap) are predictions of relativistic calculations based on the CD Bonn and AV18 potential, respectively.

a good description (see Figure 4b). Only when N^{3}LO NN chiral forces are used, a clear discrepancy between theory and data emerges in the region of A_y maximum, what is similar to the one for standard forces. Such behaviour of A_y predictions at different orders in the chiral expansion can be traced back to a high sensitivity of A_y to ^3P_j NN force components and to the fact, that only at N^{3}LO of chiral expansion the experimental ^3P_j phases [26, 27], especially the $^3P_2$-$^3F_2$ ones, are properly reproduced (see Figure 5a). Contrary to the behavior of old chiral potentials predictions, when improved chiral forces with local coordinate space regulator are applied one finds out that even at NLO A_y predictions are similar to those of standard forces. This reflects very fast convergence of phase-shifts to experimental data with order of chiral expansion for improved potentials and is exemplified for the $^3P_2$ phases in Figure 5b. Only LO phases are far away from experimental values while NLO are very close to data at energies below ≈ 40 MeV. The N^{2}LO, N^{3}LO, and N^{4}LO phases as well as the Nijmegen values overlap. The corresponding A_y predictions at orders above LO are very close together.

Using a new procedure for estimating the theoretical truncation errors introduced in [12, 13] we show in Figure 4c theoretical uncertainties in different orders for A_y predictions obtained with the improved potentials. With increasing order the uncertainties are diminishing and very precise predictions are provided at N^{3}LO and N^{4}LO. It is interesting to note that the width of the uncertainty band at N^{2}LO is of the same size as the discrepancy with respect to the data. At that order for the first time 3NF, which is neglected in the present calculations, appears. Therefore one can expect that including consistent N^{3}LO 3NF's will probably provide explanation for the A_y puzzle.

That new procedure for estimating the theoretical truncation errors provides also evidence for missing 3NF effects at higher energy elastic Nd scattering, supporting thus the results found with standard NN potentials. In Figures 6a and 6b we exemplify that in the case of the elastic scattering cross section. The expected theoretical uncertainty at N^{3}LO and N^{4}LO is substantially smaller than the observed discrepancies between calculations and data. It remains to be seen whether consistent 3NF's at N^{3}LO will explain differences found in Nd elastic scattering at higher energies.

In Figures 7 and 8 we compare predictions of improved chiral potentials at different orders to the cross section data of the proton-proton quasi-free-scattering (QFS) and the symmetric-space-star (SST) complete configurations of the deuteron breakup at two incoming nucleon energies $E =$ 13 MeV and 65 MeV. For both geometries at 65 MeV the theoretical uncertainty rapidly diminishes with increasing order of chiral expansion, providing very precise predictions at N^{3}LO and N^{4}LO order, which agree with the pd data. For pp QFS this is also the case at 13 MeV. Contrary to that, for SST at 13 MeV the uncertainty bands at different orders are rather narrow and the nd and pd breakup data are far away from theory. The two nd data sets come from different measurements and both reveal the similar disagreement to data. The pd data set shown in Figure 8a is supported by other SST pd breakup measurements [28] at this energy range. The calculations of the pd breakup with inclusion of the pp Coulomb force [29] revealed only very small Coulomb force effects for this configuration. Since at that energy the SST configuration is practically dominated by S-wave NN force components, the big difference between pd and nd data could suggest large charge-symmetry breaking in the $^1S_0$ partial wave. On the other hand the discrepancy to theory would imply that our knowledge of the $^1S_0$ pp and nn low energy forces is probably insufficient. It will be very difficult to explain these data by inclusion of a 3NF without introducing large charge symmetry breaking terms.

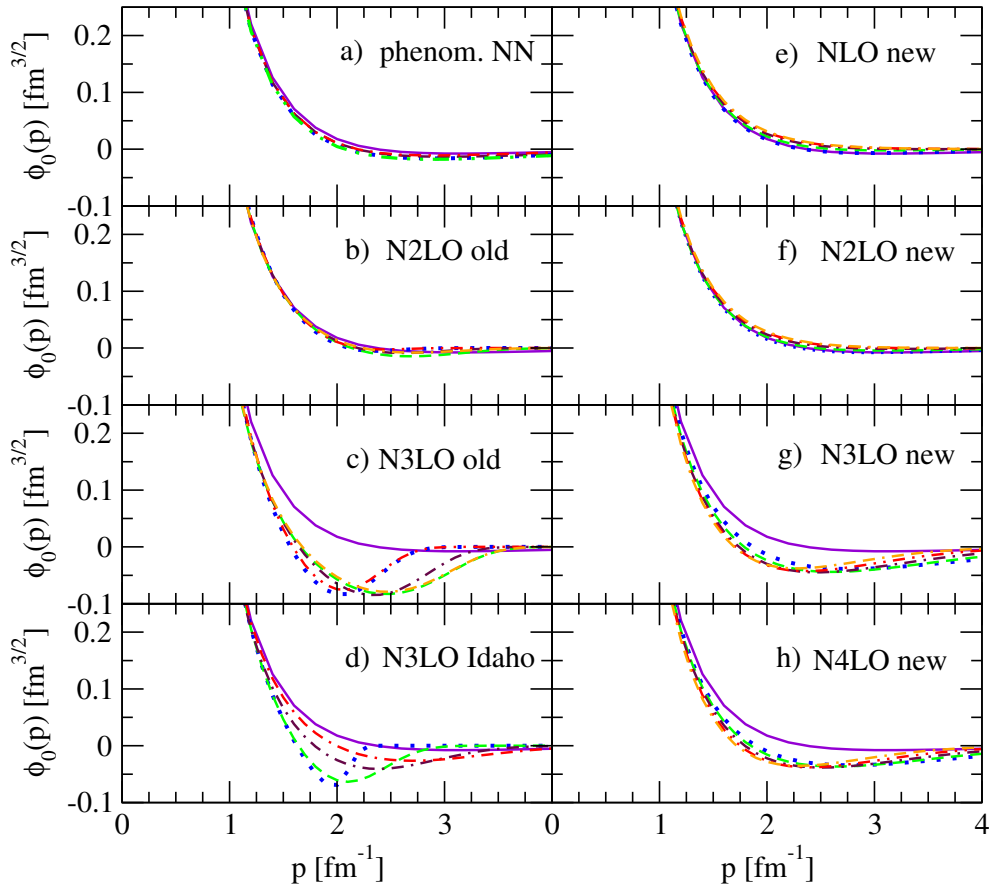

Figure 3: (Color online) The $l = 0$ deuteron wave function $\phi_0(p)$ for different NN potentials. In a) for (semi)phenomenological potentials: dotted (blue) - AV18, solid (violet) - CD Bonn, dashed-dotted (red) - Nijm1, dashed-double-dotted (green) - Nijm2, and dashed (maroon) - Nijm93. In b) (c)) for five versions of chiral N^{2}LO (N^{3}LO) potentials of Ref. [6, 7], which correspond to different cut-off values used for the Lippmann-Schwinger equation and spectral function regularizations, namely: $(450,500)$ MeV dotted (blue), $(450,700)$ MeV dashed (green), $(550,600)$ MeV dashed-dotted (maroon), $(600,500)$ MeV dashed-double-dotted (red), and $(600,700)$ MeV double-dashed-dotted (orange). In d) for four versions of chiral N^{3}LO potentials of Ref. [8] with cut-off parameters: 414 MeV dotted (blue) line, 450 MeV dashed (green) line, 500 MeV dashed-dotted (marron) line, 600 MeV double-dashed-dotted (red) line. In e)-h) for five versions of improved chiral NN potentials of Refs. [12, 13] with local regulator and parameter $R = 0.8$ fm (dotted (blue)), $R = 0.9$ fm (dashed (green)), $R = 1.0$ fm (dashed-dotted (maroon)), $R = 1.1$ fm (dashed-double-dotted (red)), $R = 1.2$ fm (double-dashed-dotted (orange)), are shown. For comparison in b)-h) also the CD Bonn wave function is shown by solid (violet) line.

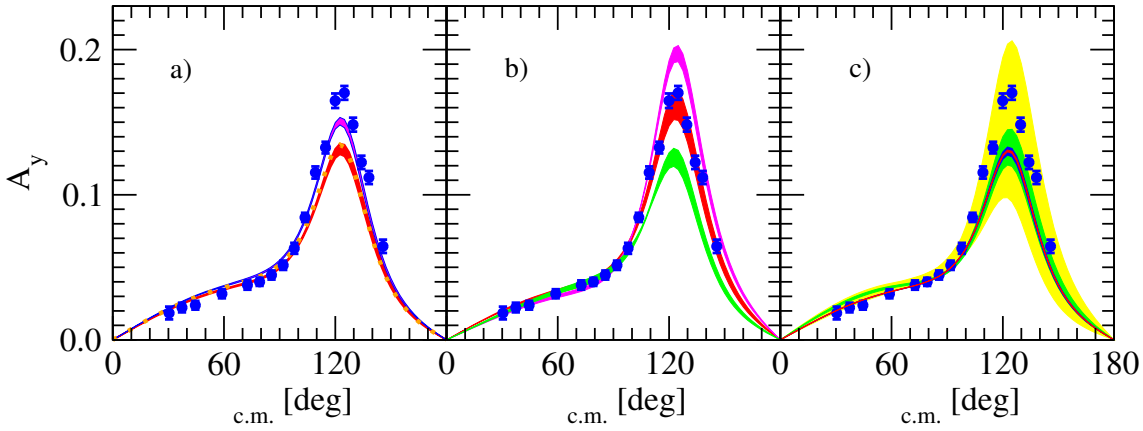

Figure 4: (Color online) The nd elastic scattering analyzing power A_y at $E_{lab} = 10$ MeV. For description of bands and lines in a) see Figure 2a. In b) bands of predictions for five versions of the old Bochum chiral NN potentials of Ref. [7] at different orders of the chiral expansion are shown: NLO - the upper (magenta) band, N^{2}LO - the middle (red) band, and N^{3}LO - the bottom (green) band. These five versions correspond to different cut-off values used for the Lippmann-Schwinger equation and spectral function regularizations, namely $(450,500)$ MeV, $(450,700)$ MeV, $(550,600)$ MeV, $(600,500)$ MeV, and $(600,700)$ MeV [7]. In c) predictions based on improved chiral NN potentials of Refs. [12, 13] with local regulator and parameter $R = 1.0$ fm are shown. The bands of increasing width show estimated theoretical uncertainty at N^{4}LO (red), N^{3}LO (blue), N^{2}LO (green) and NLO (yellow). The full circles are nd data from Ref. [32].

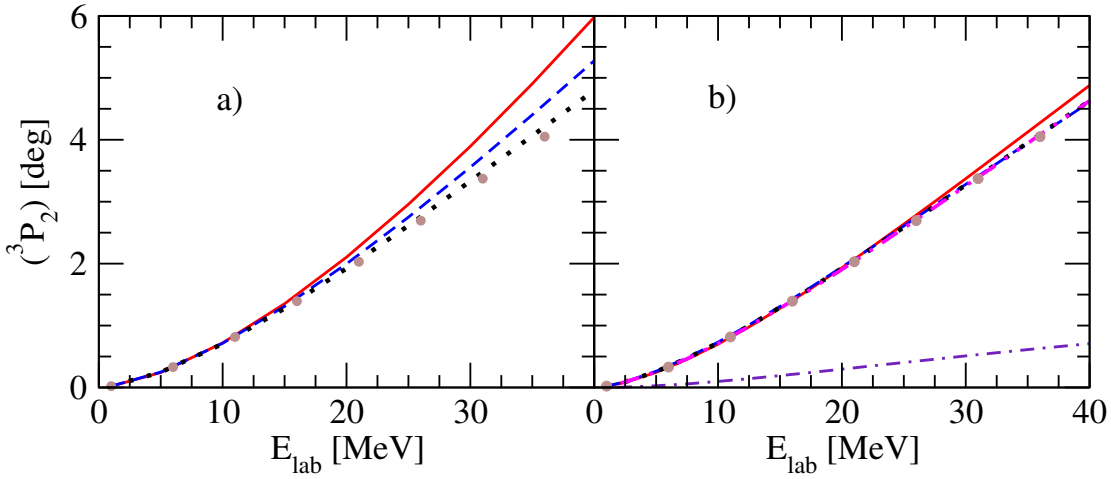

Figure 5: (Color online) The neutron-proton $^3P_2$ phase-shifts as a function of lab. energy E_{lab}. In a) the solid (red), dashed (blue), and dotted (black) lines show predictions of the old chiral Bochum NLO, N^{2}LO, and N^{3}LO NN potentials with a set of (600,500) MeV cut-off parameters. In b) the dashed-dotted (indigo), solid (red), dashed (blue), dotted (black), and dashed-double-dotted (magenta) lines are predictions of improved chiral potentials with local regulator and parameter $R = 1.0$ fm at LO, NLO, N^{2}LO, N^{3}LO, and N^{4}LO, respectively. The solid (brown) circles are experimental Nijmegen phase-shifts [26, 27].

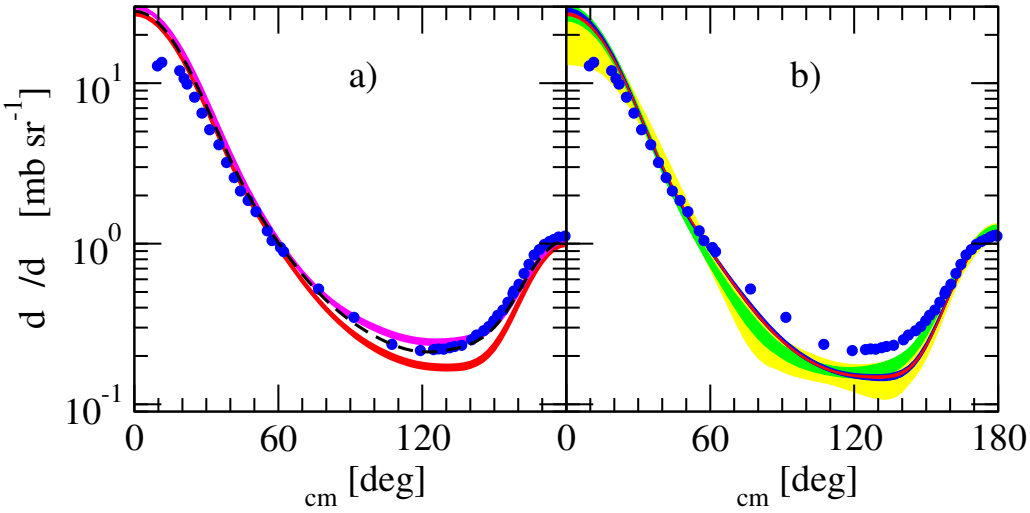

Figure 6: (Color online) The angular distribution for nd elastic scattering at neutron lab. energy $E_{lab} =$ 135 MeV. The nd experimental data (solid dots) are from [30]. In a) the light shaded (red) and dark shaded (magenta) bands result from predictions of (semi)phenomenological potentials (AV18, CD Bonn, Nijm1, Nijm2) alone and combined with TM99 3NF [23], respectively. The dashed (black) line is the prediction of the AV18+UIX 3NF. In b) predictions based on chiral NN potentials of Refs. [12, 13] for $R = 1.0$ fm are shown. The bands of increasing width show estimated theoretical uncertainty at N^{4}LO (red), N^{3}LO (blue), N^{2}LO (green) and NLO (yellow).

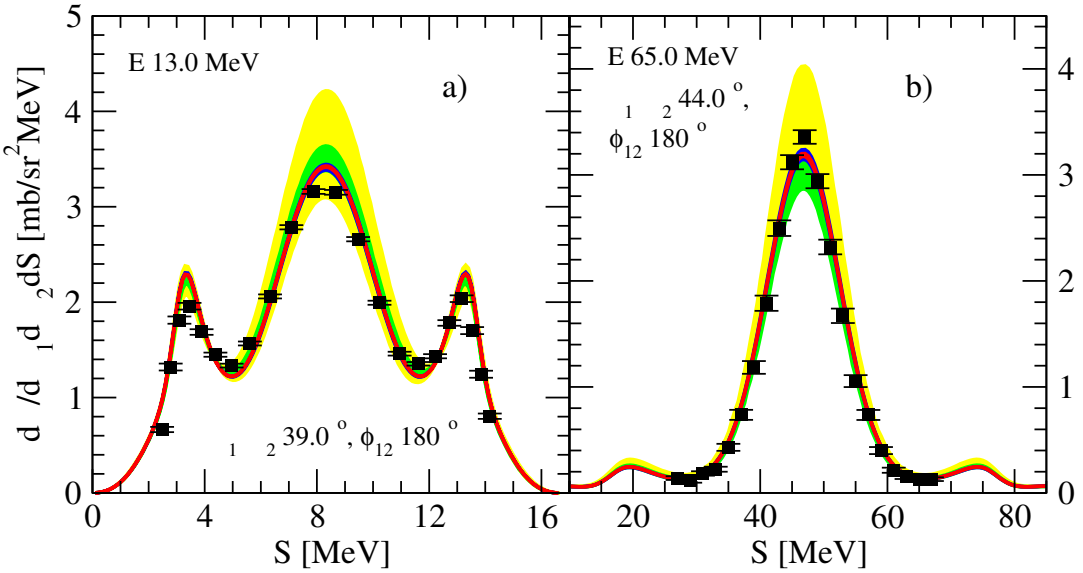

Figure 7: (Color online) The pp QFS pd breakup cross section at incoming neutron lab. energy $E_{lab} =$ 13 MeV (a)) and 65 MeV (b)), as a function of the arc-length S along the kinematical locus in the $E_1 - E_2$ plane. The bands of increasing width show estimated theoretical uncertainty at N^{4}LO (red), N^{3}LO (blue), N^{2}LO (green) and NLO (yellow) based on improved chiral NN potentials of Refs. [12, 13] with local regulator and parameter $R = 1.0$ fm. In a) the (black) squares are pd data of Ref. [33] and in b) pd data of Ref. [34].

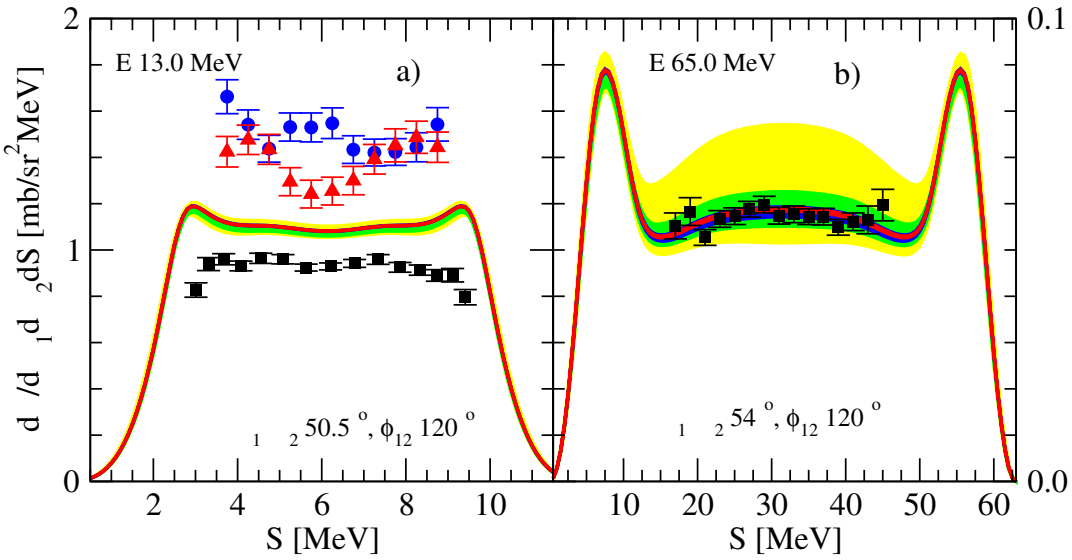

Figure 8: (Color online) The SST nd breakup cross section at incoming neutron lab. energy $E_{lab,} = 13$ MeV (a)) and 65 MeV (b)), as a function of the arc-length S along the kinematical locus in the $E_1 - E_2$ plane. The bands of increasing width show estimated theoretical uncertainty at N^{4}LO (red), N^{3}LO (blue), N^{2}LO (green) and NLO (yellow) based on improved chiral NN potentials of Refs. [12, 13] with local regulator and parameter $R = 1.0$ fm. In a) the (blue) circles and (red) triangles are nd data from Ref. [31] and [35, 36], respectively. The (black) squares are pd data of Ref. [33]. In b) the (black) squares are pd data of Ref. [37].

5. Summary

Solving 3N scattering exactly in a numerical sense up to energies below the pion production threshold allows one to test the 3N Hamiltonian based on modern NN potentials and 3NF's. At the higher energies for some observables large 3NF effects are predicted when using (semi)phenomenological models such as TM and Urbana IX. Some Nd elastic scattering cross sections and polarization data support these predictions. In some other cases, however, defects of the (semi)phenomenological 3NF's are demonstrated. Relativistic effects are found to be small for the elastic scattering cross section and negligible for spin-observables at higher energies. The discrepancies at high energies, which remain even when Urbana IX or TM 3NF's are included, point to the importance of short-range contributions to the 3NF. Application of improved chiral NN interactions up to N^{4}LO order of chiral expansion and estimation of theoretical uncertainties due to the truncation of higher orders supports conclusions obtained with standard NN potentials. Higher order chiral 3NF's comprises a number of shorter-range terms. It can be expected that an application of consistent chiral NN and 3N forces will play an important role in understanding of elastic scattering and breakup reactions at higher energies.

References

[1] R. B. Wiringa, V. G. J. Stoks, R. Schiavilla, Phys. Rev. C**51**, 38 (1995).

[2] R. Machleidt, Phys. Rev. C**63**, 024001 (2001).

[3] V. G. J. Stoks et al., Phys. Rev. C**49**, 2950 (1994).

[4] B. S. Pudliner et al., Phys. Rev. C**56**, 1720 (1997).

[5] S. A. Coon et al., Nucl. Phys. **A317**, 242 (1979).

[6] E. Epelbaum et al., Nucl. Phys. **A747**, 362 (2005).

[7] E. Epelbaum, Prog. Part. Nucl. Phys. **57**, 654 (2006)

[8] R. Machleidt and D.R. Entem, Phys. Rep.**503**, 1 (2011).

[9] E. Epelbaum et al., Phys. Rev. C**66**, 064001 (2002).

[10] V. Bernard *et al.*, Phys. Rev. C**77**, 064004 (2008).

[11] V. Bernard *et al.*, Phys. Rev. C**84**, 054001 (2011).

[12] E. Epelbaum, H. Krebs and U.-G. Meißner, Eur. Phys. J. A **51**, no. 5, 53 (2015).

[13] E. Epelbaum, H. Krebs and U.-G. Meißner, arXiv:1412.4623 [nucl-th].

[14] D. Hüber et al., Acta Phys. Polon. **B28**, 167 (1997).

[15] W. Glöckle et al., Phys. Rep.**274**, 107 (1996).

[16] H. Witała et al., Phys. Rev. C**63**, 024007 (2001).

[17] H. Witała et al., Phys. Rev. Lett. **81**, 1183 (1998).

[18] K. Sekiguchi et al., Phys. Rev. C **79**, 054008 (2009).

[19] E. Stephan et al., Eur. Phys. Journal A **42**, 13 (2009).

[20] H. Witała et al., Phys. Rev. C **71**, 054001 (2005).

[21] H. Witała et al., Phys. Rev. **C 77**, 034004 (2008).

[22] H. Witała et al., J. Phys. G **41**, 094011 (2014).

[23] S. A. Coon and H. K. Han, Few-Body Systems **30**, 131 (2001).

[24] W. Abfalterer et al., Phys. Rev. Lett. **81**, 57 (1998).

[25] Y. Maeda et al., Phys. Rev. C **76**, 014004 (2007).

[26] J. R. Bergervoet et al., Phys. Rev. C**41**, 1435 (1990).

[27] V.G.J. Stoks et al., Phys. Rev. C**48**, 792 (1993).

[28] K. Sagara, Few-Body Systems **48**, 59 (2010).

[29] A. Deltuva, A.C. Fonseca, and P.U. Sauer, Phys. Rev. C**72**, 054004 (2005).

[30] H. Sakai et al., Phys. Rev. Lett. **84**, 5288 (2000).

[31] H. R. Setze et al., Phys. Lett. **B388**, 229 (1996).

[32] W. Tornow et al., Phys. Rev. Lett. **49**, 312 (1982).

[33] G. Rauprich et al. Nucl. Phys. **A535**, 313 (1991).

[34] M.Allet et al., Few-Body Systems **20**, 27 (1996).

[35] J. Strate et al., J. Phys. G: Nucl. Phys. **14**, L229 (1988).

[36] J. Strate et al., Nucl. Phys. **A501**, 51 (1989).

[37] J. Zejma et al, Phys. Rev. C**55**, 42 (1997).